NUMERICAL DETERMINATION OF DIFFUSION COEFFICIENTS IN WOOD USING DATA FROM CT-SCANNING

John Eriksson
Ph.D. Student

Håkan Johansson
Ph.D.
Department of Applied Mechanics
Chalmers University of Technology
SE-412 96 Göteborg, Sweden

and

Jonas Danvind
Ph.D. Student
Valutec AB
Box 709
SE-931 27 Skellefteå, Sweden

(Received February 2005)

ABSTRACT

The radial moisture diffusion coefficient in Fick's law for a sample of Norway spruce (*Picea abies*) under isothermal drying conditions was determined in a parameterization of Arrhenius' equation type. Using X-ray CT-scanning, the wood density and moisture content distributions were obtained in the radial direction for the wood sample. An optimization scheme, based on finite element computation, was then applied to find the parameter values such that the difference between observed and computed moisture content was minimized. The combined numerical and experimental technique was developed to reduce known disadvantages of similar approaches, and a specific algorithm to determine diffusion coefficients was presented. A comparison of the calibrated diffusion coefficient with those given in the literature showed a good fit. The computed moisture content based on the obtained diffusion coefficient and the observed moisture content agreed well. Finally, the effect of measurement errors on the computed material parameter was found to be small.

Keywords: Calibration, CT-scanning, diffusion coefficient, parameter identification, wood drying.

INTRODUCTION

A diversity of models based on either diffusion, empiricism, or phase separation mechanisms has been developed for analyzing drying of timber. Keey et al. (2000) provide an overview. When studying drying that occurs under isothermal conditions below the fiber saturation point, unsteady-state diffusion models have frequently been applied. For such a simplified approach to work well, the need for good material data is vital. Different experimental techniques, such as the cup or the sorption method combined with analytical or numerical solutions, have been applied to resolve the material properties. In the determination procedure, there exist numerous difficulties, such as non-Fickian behavior, e.g. apparently sample-length dependency of the diffusion coefficients and material parameters that display a significant dependence upon the magnitude of step change in relative humidity (Wadsö 1993). Other difficulties are the influence of surface resistance, the effect of sorption hysteresis, the moisture dependency of the diffusion coefficients, and the restrictions of us-

ing analytical solutions in the determination process.

To overcome some of the shortcomings connected with traditional techniques, Olek and Weres (2001) point out that a so-called inverse method appears to be a valuable tool for determining the coefficients. In particular, the method does not put restraints on the boundary conditions or initial moisture distribution in the sample. In fact, Koc et al. (2003) use an inverse method to study surface resistance. Inverse identification in terms of a numerical technique for an underlying equation of state in conjunction with the minimization of an objective function has been successfully applied by Chen at al. (1996) and Simpson and Liu (1997) to evaluate the diffusion coefficient in yellow poplar and red oak, respectively. These papers, however, are somewhat unclear regarding the particular choice of optimization technique used to find the minimum of the objective function. Another approach, employed in Liu et al. (2001), is to first via "inverting" the state equation, determine the diffusion coefficient as a function in space and time, and thereby obtain a relatively standard least squares problem. This approach seems promising, but is not further discussed in this paper.

Inverse problems are often described as ill-posed, and for this reason sensitive to measurement errors (Olek and Weres 2001). An attempt to achieve better conditioning of the problem is made in this paper by combining the advantages of the inverse approach with a sophisticated measurement technique. The particular combination adopted has shown promising results in a preliminary study (Danvind et al. 2004). Moreover, the computational and experimental techniques presented are developed to reduce certain disadvantages of the inverse technique listed in (Liu et al. 2001).

The aim of this paper is to derive a specific scheme for the inverse problem in the context of diffusion by using a recently proposed mathematical framework for parameter identification (Johansson and Runesson 2005). Here, the radial moisture diffusion coefficient in Fick's law for samples of Norway spruce sapwood under isothermal drying conditions is determined. By means of X-ray Computed Tomography (CT) scanning, it is possible to accurately determine the density distributions and moisture content (MC) in wood samples. Based on these experimental data and computed results from finite element (FE) simulations, an optimization scheme is used to minimize the difference between observed and computed MC. An advantage to using this approach is that difficult surface measurements and the introduction of assumptions concerning the surface resistance are evaded. In the literature, several parameterizations describing the diffusion coefficient dependencies are proposed and each involves a set of parameter values, cf. Koponen (1984), Hukka (1999), and Keey et al. (2000). The combination of optimization technique and an Arrhenius equation-type parameterization has been shown capable of describing internal moisture transfer coefficients during drying in red oak (Simpson and Liu 1997) and for this reason is used in this study. Nevertheless, the implementation of any other parameterization is straightforward. Finally, the sensitivity of the optimization problem, i.e. the effects of measurement errors on the computed material parameters, is studied.

THEORETICAL BACKGROUND

The moisture transport in wood below the fiber saturation point may be described with a diffusion-type partial differential equation in space-time, whereby $x \in \Omega$ and $t \in I = (0,T)$ denote space and time coordinates, respectively. The diffusion coefficient in the radial direction is denoted $D_r(\underline{p},\omega)$, indicating its dependence on the moisture content $\omega(x,t)$ [kg/m^3], and a set of parameter values denoted by $\underline{p}$. For brevity, the subscript r is dropped henceforth. The governing state equation is in the one-dimensional case assuming constant cross-section

$$\frac{\partial \omega}{\partial t} - \frac{\partial}{\partial x}\left(D(\underline{p},\omega)\frac{\partial \omega}{\partial x}\right) = 0 \quad x \in \Omega$$
$$\omega = \omega_D, x \in \partial\Omega_D, \quad \text{and} \quad q_n = h, x \in \partial\Omega_h \tag{1}$$

with the initial condition $\omega(x,0) = \omega_0$, the domain of interest being referred to as Ω and corresponding boundaries being denoted by $\partial\Omega = \partial\Omega_D \cup \partial\Omega_h$. In Eq. (1), q_n denotes prescribed flow, while ω_D refers to prescribed moisture content. The aim is to find the values of the material parameters $\underline{p}$ that give the optimal fit between predicted and measured values of the moisture content. This aim can be formulated as a constrained optimization problem: Find $\underline{p}$ such that the objective function

$$\mathcal{F} = \frac{1}{2}\sum_{i=1}^{N^{OBS}} c_i(\omega_i(\bar{x}_i,\bar{t}_i) - \omega_i^{OBS})^2 \qquad (2)$$

for measured values ω_i^{OBS} at specific coordinates $x = \bar{x}_i$ and times $t = \bar{t}_i$ with a weight factor c_i (here $c_i = 1/N^{OBS}$) is minimized under the constraint that $\underline{p}$ and ω satisfy Eq. (1). It is noted that, in order to evaluate $\mathcal{F}$ for given values of $\underline{p}$, the solution of the state Eq. (1) is needed to obtain ω. The formulation of the objective function Eq. (2) has the specific advantage of decoupling the numerical method needed to solve the state Eq. (1) from the experimental data. In particular, it implies that neither the spatial nor the temporal discretization needs to coincide with points $(\bar{x}_i,\bar{t}_i)$ in space-time where the MC is measured. This important feature gives the flexibility to choose discretization such that desired accuracy of the results is ensured.

There are numerous general optimization procedures for minimizing a function under equality constraints. Commonly, these methods are divided into gradient-based and non-gradient methods, where the latter do not need analytical derivatives of the objective function. In general, non-gradient methods are more likely of finding the global minimum among many local ones but also tend to need a greater number of evaluations of $\mathcal{F}$. Each such evaluation involves the solution of a FE problem and is therefore computationally expensive. Thus, a gradient-based method is preferred here. The concept of parameter identification in terms of optimization is discussed in Mahnken (1998).

To overcome the difficulties involved in finding analytical expression for the derivative of $\mathcal{F}$ with respect to $\underline{p}$ (while the equality constraint Eq. (1) is satisfied), either the direct differentiation or the adjoint system method can be employed (cf. Kleiber et al. 1997). Here, the adjoint system method expressed in terms of a Lagrangian function will be used. Furthermore, the derivation of the optimization scheme will be carried out in a finite element setting. Equation (1) must then be expressed in terms of FE-equations in space as well as in time. To this end, the time interval $I = (0,T)$ of interest is divided into a number of discrete segments denoted by I_n with length $\Delta t_n = t_n - t_{n-1}$, such that the weak form of the state equation associated with the time interval n is (Eriksson et al. 1996)

$$\int_\Omega \left(\int_{I_n} \left(\frac{\partial \omega}{\partial t} v + D \frac{\partial \omega}{\partial x}\frac{\partial v}{\partial x} \right) dt + (\omega(t_{n-1}^+) - \omega(t_{n-1}^-))v(t_{n-1}^+) \right) d\Omega = 0 \qquad (3)$$

$\forall v \in V_n^0$, $n = 1, 2, \ldots, N$ where V_n^0 is a suitable test space associated with the time step n (the superscripts acting on t are illustrated in Fig. 1). A finite element discretization corresponding to cG(1)dG(0) is introduced, i.e. the approximated solution $\omega_h(x,t)$ is piecewise linear and continuous in space and piecewise constant (thus, discontinuous) in time. The function $\omega_h(x,t)$ is represented by nodal values $\mathbf{W}$, linear basis (shape) functions $\mathbf{N}_x(x)$ in space, and constant basis functions $\mathbf{N}_t(t)$ in time. The spatial-temporal moisture field may then be expressed by

$$\omega(x,t) \approx \omega_h(x,t) = \mathbf{N}_x(x)\mathbf{N}_t(t)\mathbf{W} \qquad (4)$$

Since $\mathbf{N}_t(t)$ is piecewise constant in time with support only at a specific time subintervals I_n, it is noted that the time integration in Eq. (3) may be carried out using that

$$\int_0^T \omega(x,t)dt = \Delta t_n \mathbf{N}_x(x)\mathbf{W}_{[n]} = \Delta t_n \mathbf{N}(x)\mathbf{W}_{[n]} \qquad (5)$$

where the subscript on the spatial basis functions has been dropped and, as can be seen in the above equation, the nodal values have been

put into a time-dependent vector as $\mathbf{W} = [\mathbf{W}_{[1]}{}^T, \mathbf{W}_{[2]}{}^T, \ldots, \mathbf{W}_{[N]}{}^T]^T$ to simplify subsequent notations. It is noted that the specific choice of discretization both in space as well as time, contrary to a recurrence scheme in time, implies that the time derivative is acting on the shape function. Recalling piecewise constant approximation in time, thus $\dot{\mathbf{N}}_t = 0$, the dot denoting the time-derivative. Then, derivatives of $\omega(x,t)$ can be expressed in terms of nodal values and basis functions as

$$\frac{\partial \omega(x,t)}{\partial t} \approx \dot{\mathbf{N}}_t(t)\mathbf{N}_x(x)\mathbf{W} = 0,$$
$$\left.\frac{\partial \omega}{\partial x}\right|_t \approx \mathbf{B}\mathbf{W}_{[n]}, \quad t \in I_n = (t_{n-1}, t_n) \tag{6}$$

The finite element format of Eq. (3) can be obtained using Eq. (5) and Eq. (6)

$$\int_\Omega (\Delta t_n D \mathbf{B}^T \mathbf{B}\mathbf{W}_{[n]} - \|\omega_h\|_{n-1}\, \mathbf{N}^T) d\Omega = \mathbf{0}$$
$$n = 1,2,\ldots,N \tag{7}$$

where $\|\omega_h\|_{n-1} = \boldsymbol{\omega}_h(x,t_{n-1}^+) - \boldsymbol{\omega}_h(x,t_{n-1}^-) = \mathbf{N}(\mathbf{W}_{[n]} - \mathbf{W}_{[n+1]})$ denotes the discontinuity (jump) that can arise at the discrete time-nodes in the approximations, (see Fig. 1). Returning to the minimization problem, the Lagrangian $\mathcal{L}$ is obtained by adding the constraint Eq. (3), using the Lagrangian multiplier λ as a test function, to Eq. (2). It is noted that $\lambda \in V_n^0$ and, consequently, a

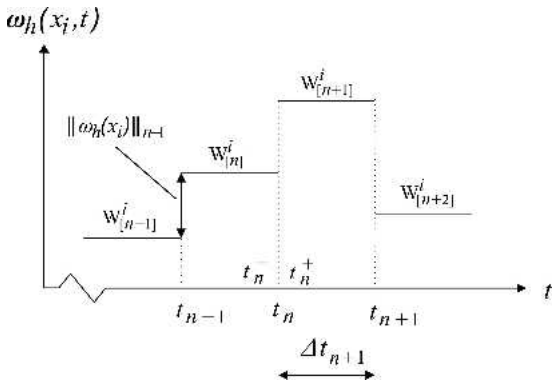

FIG. 1. Principal illustration of the temporal approximation in dG(0) where W^i is interpolated at a position x_i from $\mathbf{W}$.

FE-approximation of λ is introduced in analogy to Eq. (4) and Eq. (6) as

$$\lambda \approx \lambda_h = \mathbf{N}\boldsymbol{\Lambda}, \quad \frac{\partial \lambda}{\partial t} \approx \dot{\mathbf{N}}\boldsymbol{\Lambda} = 0, \quad \left.\frac{\partial \lambda}{\partial x}\right|_t \approx \mathbf{B}\boldsymbol{\Lambda}_{[n]} \tag{8}$$

where $\boldsymbol{\Lambda} = [\boldsymbol{\Lambda}_{[1]}^T, \boldsymbol{\Lambda}_{[2]}^T, \ldots, \boldsymbol{\Lambda}_{[N]}^T]^T$ contains nodal values of the discretized Lagrangian multiplier (λ_h). Then, the Lagrangian may be expressed in FE-format in terms of contributions from each time subinterval as

$$\mathcal{L}(\underline{p},\omega_h,\lambda_h) = \sum_{n=1}^{N} \mathcal{L}_{[n]}(\underline{p},\omega_h,\lambda_h) \tag{9}$$

$$\mathcal{L}_{[n]} = \frac{1}{2}\sum_{i\in\Im_n} c_i(\mathbf{N}(\bar{x}_i)\mathbf{W}_{[n]} - \omega_i^{OBS})^2 + \int_\Omega \Delta t_n D\, \mathbf{W}_{[n]}^T \mathbf{B}^T \mathbf{B}\boldsymbol{\Lambda}_{[n]} d\Omega + \int_\Omega \|\omega_h\|_{n-1}\, \mathbf{N}\boldsymbol{\Lambda}_{[n]} d\Omega \tag{10}$$

where $\Im_n = \{i : \bar{t}_i \in I_n\}$. A key property of the Lagrangian formulation is that it allows $\underline{p}$, ω_h, and λ_h to be treated as independent; in particular, ω_h is not a function of $\underline{p}$. The non-fulfilment of the state equation is embedded in the Lagrangian multiplier, λ_h, which may be viewed upon as an extra state field (costate). Then, from the construction of $\mathcal{L}$, a minimum of $\mathcal{F}$ corresponds to a stationary point of $\mathcal{L}$, i.e., the derivatives with respect to $\mathbf{P}$, $\mathbf{W}$, and $\boldsymbol{\Lambda}$ are zero, $\mathbf{P}$ being the vector representation of the set of material parameters $\underline{p}$. Thus, $\underline{p}$, ω_h and λ_h are sought such that the residuals, $\mathbf{r}_p = -\mathcal{L}'_p$ etc., vanish for all $n = 1,2,\ldots,N$. This yields

$$\mathbf{r}_p = -\sum_{n=1}^{N} \Delta t_n \int_\Omega \mathbf{D}'_p (\mathbf{W}_{[n]}^T \mathbf{B}^T \mathbf{B}\boldsymbol{\Lambda}_{[n]}) d\Omega \tag{11}$$

$$\mathbf{r}_{\omega[n]} = -\sum_{i\in\Im_n} c_i(\mathbf{N}(\bar{x}_i)\mathbf{W}_{[n]} - \omega_i^{obs})\mathbf{N}^T(\bar{x}_i) - \int_\Omega \Delta t_n (D'_\omega \mathbf{W}_{[n]}^T \mathbf{B}^T \mathbf{B}\boldsymbol{\Lambda}_{[n]}) \mathbf{N}^T d\Omega - \int_\Omega \Delta t_n D \mathbf{B}^T \mathbf{B}\boldsymbol{\Lambda}_{[n]} d\Omega + \int_\Omega \|\lambda_h\|_n \mathbf{N}^T d\Omega \tag{12}$$

$$\mathbf{r}_{\lambda[n]} = -\int_{\Omega} \Delta t_n D\mathbf{B}^T\,\mathbf{B}\mathbf{W}_{[n]} d\Omega - \int_{\Omega} \|\omega_h\|_{n-1}\mathbf{N}^T d\Omega \tag{13}$$

The derivative of the last term in Eq. (10) with respect to **W** yields also a contribution to the previous time interval n-1; however, taking this into account recursively allows the corresponding term in Eq. (12) to be expressed as a jump in λ_h. Furthermore, Eq. (7) appears again as Eq. (13) and, hence, the governing state equation will be satisfied when a stationary point of $\mathcal{L}$ is found. The notation $\mathbf{r}_\omega = [\mathbf{r}_{\omega[1]}{}^T, \mathbf{r}_{\omega[2]}{}^T, \ldots, \mathbf{r}_{\omega[N]}{}^T]^T$ is used to collect the components from all time steps in a vector in the same way as for **W** and **Λ**, $\mathbf{r}_\lambda$ being defined analogously. Further, introducing a short notation via a vector **Z** containing the unknowns $\mathbf{Z} = [\mathbf{P}^T, \mathbf{W}^T, \mathbf{\Lambda}^T]^T$ and the residual vector $\mathbf{r} = [\mathbf{r}_p^T, \mathbf{r}_\omega^T, \mathbf{r}_\lambda^T]^T$, Eqs. (11)–(13) may be expressed as a set of nonlinear equations

$$\mathbf{r}(\mathbf{Z}) = \mathbf{0} \tag{14}$$

which is to be solved by means of a Newton-type method where an update $d\mathbf{Z}$ is solved for from the linear system

$$\mathbf{K}^{(k)} d\mathbf{Z} = \mathbf{r}^{(k)} \tag{15}$$

involving **K** as the derivative of $-\mathbf{r}(\mathbf{Z})$ with respect to **Z** and thus, obtain the new iterate as

$$\mathbf{Z}^{(k+1)} = \mathbf{Z}^{(k)} + \alpha d\mathbf{Z} \tag{16}$$

where α is a step length chosen such that the merit function in Euclidian norm

$$M(\alpha) = \text{norm}(\mathbf{r}(\mathbf{Z}^{(k)} + \alpha d\mathbf{Z})) \tag{17}$$

is minimized, or, in practice, reduced. The merit function Eq. (17) is needed to ensure convergence and plays the role of a line search procedure, (cf. Luenberger (2003). It is noted that as $\mathbf{Z}^{(k)}$ closes to the optimum, α tends to unity. The procedure of computing a direction from the linear system Eq. (15), computing a step length α by minimizing Eq. (17), and computing the new **Z** from Eq. (16) is repeated until an optimality criterion is met, in most practical situations $\text{norm}(\mathbf{r}(\mathbf{Z}^{(k)})) < tol$. Then, the optimal set of material parameters $\underline{p}$, as well as the moisture content distribution ω_h, can be extracted from **Z**. Unfolding the very compact notation **K**, a more explicit version of Eq. (15) becomes

$$\begin{bmatrix} \mathbf{K}_{pp} & \mathbf{K}_{p\omega} & \mathbf{K}_{p\lambda} \\ \mathbf{K}_{p\omega}^T & \mathbf{K}_{\omega\omega} & \mathbf{K}_{\omega\lambda} \\ \mathbf{K}_{p\lambda}^T & \mathbf{K}_{\omega\lambda}^T & \mathbf{K}_{\lambda\lambda} \end{bmatrix}^{(k)} \begin{bmatrix} d\mathbf{P} \\ d\mathbf{W} \\ d\mathbf{\Lambda} \end{bmatrix} = \begin{bmatrix} \mathbf{r}_p \\ \mathbf{r}_\omega \\ \mathbf{r}_\lambda \end{bmatrix}^{(k)} \tag{18}$$

where the components are second derivatives of the Lagrangian Eqs. (9)–(10) as

$$\mathbf{K}_{pp} = \sum_{n=1}^{N} \int_{\Omega} \Delta t_n (\mathbf{W}_{[n]}^T \mathbf{B}^T\,\mathbf{B}\mathbf{\Lambda}_{[n]}) \mathbf{D}''_{pp}\, d\Omega \tag{19}$$

$$\mathbf{K}_{p\omega[n]} = \int_{\Omega} \Delta t_n [(\mathbf{W}_{[n]}^T \mathbf{B}^T\,\mathbf{B}\mathbf{\Lambda}_{[n]}) \mathbf{D}''_{p\omega}\mathbf{N} + (\mathbf{B}\mathbf{\Lambda}_{[n]}) \mathbf{D}'_p \mathbf{B}] d\Omega \tag{20}$$

$$\mathbf{K}_{p\lambda[n]} = \int_{\Omega} \Delta t_n (\mathbf{B}\mathbf{W}_{[n]}) \mathbf{D}'_p \mathbf{B}\, d\Omega \tag{21}$$

$$\mathbf{K}_{\omega\omega[n,n]} = \sum_{i \in \Im_n} \mathbf{N}^T(\bar{x}_i)\mathbf{N}(\bar{x}_i) + \int_{\Omega} \Delta t_n [(\mathbf{D}''_{\omega\omega}\mathbf{W}_{[n]}^T \mathbf{B}^T\,\mathbf{B}\mathbf{\Lambda}_{[n]})\mathbf{N}^T\mathbf{N} + (D'_\omega \mathbf{B}\mathbf{\Lambda}_{[n]})\mathbf{B}^T\mathbf{N} + (D'_\omega \mathbf{B}\mathbf{\Lambda}_{[n]})\mathbf{N}^T\mathbf{B}] d\Omega \tag{22}$$

$$\mathbf{K}_{\omega\lambda[n,n]} = \int_{\Omega} \Delta t_n [(D'_\omega \mathbf{W}_{[n]}^T \mathbf{B}^T)\mathbf{N}^T\mathbf{B} + D\mathbf{B}^T\mathbf{B}] + \mathbf{N}^T\mathbf{N}\, d\Omega \tag{23}$$

$$\mathbf{K}_{\omega\lambda[n,n+1]} = -\int_{\Omega} \mathbf{N}^T\mathbf{N}\, d\Omega \tag{24}$$

Similarly to $\mathbf{r}_\omega$ and $\mathbf{r}_\lambda$, the matrices $\mathbf{K}_{p\omega}$ and $\mathbf{K}_{p\lambda}$ consist of the contributions $\mathbf{K}_{p\omega[n]}$ and $\mathbf{K}_{p\lambda[n]}$ associated with each time step $n = 1, 2, \ldots, N$. The square matrix $\mathbf{K}_{\omega\omega}$ is constructed by $\mathbf{K}_{\omega\omega[n,n]}$ on the diagonal while all off-diagonal terms are zero. Finally, $\mathbf{K}_{\omega\lambda}$ consists of diagonal

terms $\mathbf{K}_{\omega\lambda[n,n]}$ and superdiagonal terms $\mathbf{K}_{\omega\lambda[n,n+1]}$, representing the coupling between two adjacent time steps, while the remaining entries are zero. Figure 2 illustrates the structure of the key equation Eq. (18). The parameterization of the diffusion coefficient D is of Arrhenius' equation type; see Eq. (25), based on the work in Simpson and Liu (1997) leading to the material parameters $\mathbf{P} = [p_1, p_2]$ to be determined

$$D(\underline{p},\omega) = p_1 e^{p_2\omega} \tag{25}$$

The explicit derivatives of $D(\underline{p},\omega)$ with respect to $\underline{p}$ and ω can be obtained as

$$\mathbf{D}'_p(\underline{p},\omega) = \begin{bmatrix} e^{p_2\omega} \\ p_1\omega e^{p_2\omega} \end{bmatrix} \tag{26}$$

$$D'_\omega(\underline{p},\omega) = p_1 p_2 e^{p_2\omega} \tag{27}$$

and the second derivatives are given as

$$\mathbf{D}''_{pp}(\underline{p},\omega) = \begin{bmatrix} 0 & \omega e^{p_2\omega} \\ \omega e^{p_2\omega} & p_1\omega^2 e^{p_2\omega} \end{bmatrix} \tag{28}$$

$$\mathbf{D}''_{p\omega}(\underline{p},\omega) = \begin{bmatrix} p_2 e^{p_2\omega} \\ (1+\omega\, p_2) p_1 e^{p_2\omega} \end{bmatrix} \tag{29}$$

$$D''_{\omega\omega}(\underline{p},\omega) = p_1 p_2^2 e^{p_2\omega} \tag{30}$$

It is noted that the generalization to a 2D or 3D case is rather straightforward from the FE-format used in this paper, from the definition of $\mathcal{L}$ in Eq. (10) to the definition of the last component in $\mathbf{K}$, Eq. (24). Nevertheless, the diffusion coefficient is then no longer a scalar, and therefore, the corresponding expression of the second term in Eq. (10) would be

$$\int_\Omega \Delta t_n \, \mathbf{W}^T_{[n]} \mathbf{B}^T \mathbf{D} \mathbf{B} \mathbf{\Lambda}_{[n]} d\Omega \tag{31}$$

As a consequence, the derivatives with respect to $\mathbf{P}$ (arising in the terms $\mathbf{r}_p$, $\mathbf{K}_{pp}$, $\mathbf{K}_{p\omega}$ and $\mathbf{K}_{p\lambda}$) would then have to be expressed componentwise for each p_i.

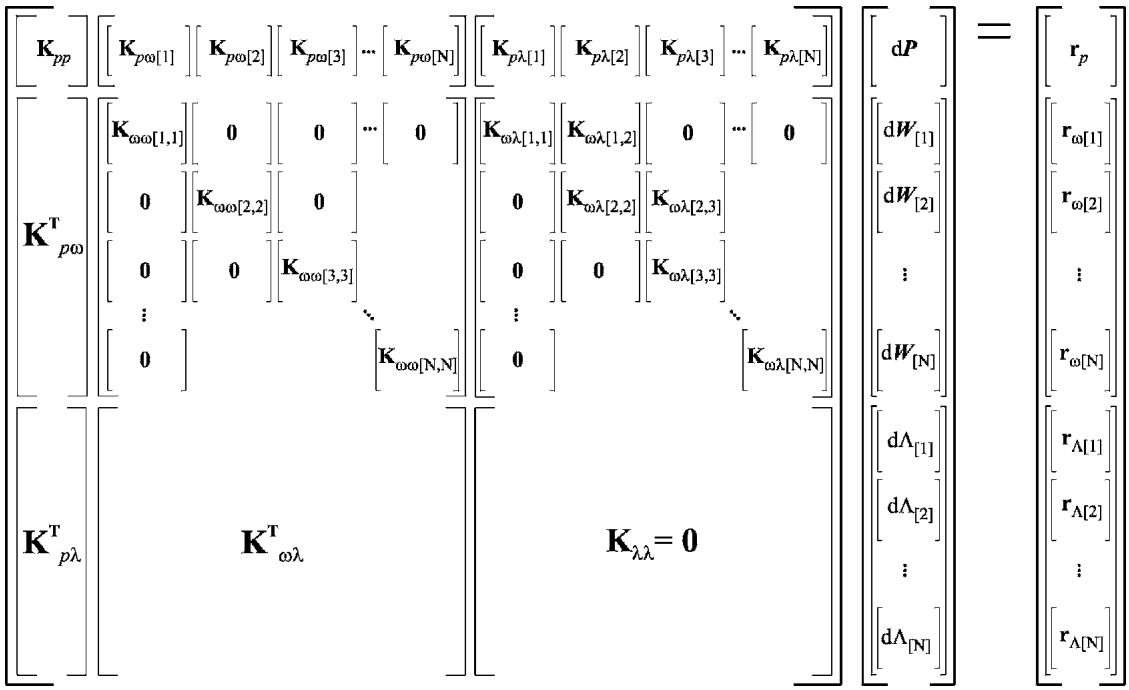

FIG. 2. Illustration of the equation system to be solved in Eq. (18).

MATERIAL AND METHOD

Experimental set-up

A clear wood Norway spruce (*Picea abies*) sample with the green dimensions of 42 × 31 × 205 mm^3 in the tangential, radial, and longitudinal direction, respectively, was dried in this study. The sample contained only sapwood, and five of its surfaces were coated using polyurethane glue (Cascol 1809 from Casco) and aluminium foil to ensure restricted drying in one dimension, (see Fig. 3). The coated surfaces were also thermally insulated using Styrofoam. During drying, the humidity and temperature of the circulating air were approximately constant at 43% H and 50°C corresponding to an equilibrium moisture content of approximately 7%, and the air speed was approximately 4 m/s. The drying from about 135% to 7% MC involves a receding wet line through the sample, but only data relevant for diffusion, about 30% MC and below, are presented further on. Every 10th minute a density image of the interior in one position was captured using a Siemens Somatom AR.T. X-ray CT scanner. Since only radial diffusion was studied, the CT-scanning was performed in the RT plane. At the end of drying, the sample was cut into five slices, and the final moisture content distribution within the sample was determined using the oven-dry method i.e. drying the sample at 103°C during 24 h. The resulting average dry density was 469 kg/m^3. By using the final MC and information on the shape of the sample and the density images, the local displacements and MC throughout the drying could be estimated by using a method presented in Danvind and Morén (2004). The method is briefly described below. Since moisture movement in one direction was to be studied, mean MCs in 2 × 30 of smaller 10 × 10 pixels regions were calculated for 10 equidistant positions in depth. These 2 × 30 regions can be seen in Fig. 3 represented as a coherent area of either (*) or (o) marks. The pixel size was 0.135 × 0.135 mm^2. The annual rings can be seen as lines drawn on top of the CT image. During the drying, the temperatures at two internal points and at the surface were also monitored. However, these are not presented here since the temperature gradient was found to be negligible over the cross-section. The sample temperature was found constant at 50°C in the diffusion regime of drying, which was studied here.

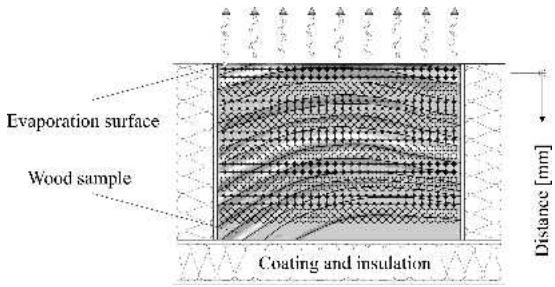

FIG. 3. Illustration of test set-up based on CT images of a Norway spruce sample cross-section in the RT plane at the end of drying. Each mark, (*) or (o), is in the center of a 10 × 10 pixels region in the original CT image, for which the MC was evaluated. Lines are drawn to form an idea of annual ring orientation.

Perturbation of moisture content

The method in Danvind and Morén (2004) used information of the boundary shape of the scanned object in CT images to estimate displacement and deformation of the studied object. Each CT image was processed to a binary image, so that object pixels were set to one and background pixels were set to zero. The relative position of a pixel in the undeformed object was calculated by studying the CT image from four corners. The position of that pixel was assumed to be at the corresponding relative position in the deformed image. By using the estimated displacements and strains in combination with measured density, the moisture content was calculated. Using a slightly different evaluation technique, Danvind (2003) found the measurement errors to be approximately a normal-distributed stochastic process with zero mean value and standard deviation (SD) 0.6% MC. It can be concluded, however, that the difference in evaluation techniques affects only quantities that have a relatively small contribution to the total error. Since the measuring volume for the test here is much larger than the one used in Danvind

(2003), 40.6 × 2.7 × 5 mm^3 versus 2 × 2 × 1.5 mm^3, the relative MC errors were expected to be smaller in the trial presented here. Also, the sample was not dried to 0% MC during the test, for determining the dry weight. Instead it was cut into five slices after the test run for determination of final MC and dry weight at different distance from the evaporation surface. Therefore, a small absolute measuring error, either lowering or raising all MC, could have been introduced due to errors in the determination of the dry density. As mentioned in the introduction, most inverse identification problems are sensitive to measurement errors. In the worst case, the diffusion coefficient predictions obtained may be overwhelmed by the noise in the experimental data. To study the sensitivity in this paper, the moisture content observed was synthetically perturbed in four steps: no disturbance SD = 0% MC (i.e. the original data), small disturbance SD = 0.3% MC, medium disturbance SD = 0.6% MC, and large disturbance SD = 0.8% MC. These perturbations affect the data that already contains the true noise from the experiment.

RESULTS AND DISCUSSION

Because of the experimental set-up, the boundary conditions are assumed to be known flux (i.e. zero) at the bottom and prescribed moisture content $\omega = \omega_D$ at the top, where ω_D is interpolated in time from data at the measurement points closest to the free surface. With ω_i^{OBS} as the remaining data from the CT-scanning, the optimization scheme described above was run for four different levels of synthetic perturbation as described earlier. The finite element discretization consisted of 30 space elements and 300 time elements. This was the appropriate element division found when computational effort was balanced with accuracy.

Figure 4 shows the iteration procedure for two of the runs. Nine iterations were required to find the optimal set of parameters without perturbation of moisture content, the last three iterations being positioned almost on top of each other and, hence, difficult to distinguish in the figure. A valley in the contour line of the objective function can be seen extending from top left and opened out at bottom right. At further right, outside the figure, the valley is closed. It appears that the developed algorithm finds the global minimum, the objective function defined in Eq. (2) being 0.677 for the undisturbed data. The optimization algorithm needed three additional iterations when the moisture content was perturbed with SD = 0.6% MC. Depending on the specific perturbation, which is a stochastic process, the number of iterations can vary some. In the particular run shown in the figure, the objective function was found to be 4.685. This means, of course, that the diffusion model can-

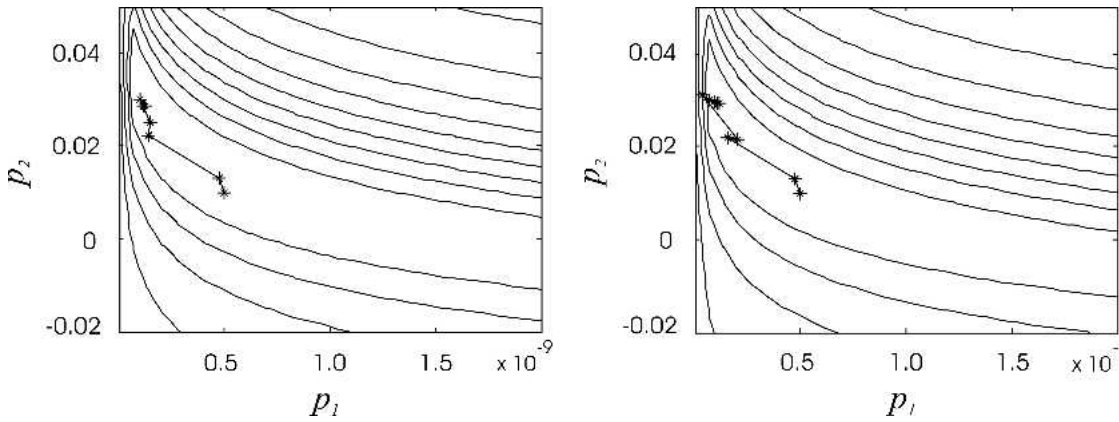

FIG. 4. Contour lines of $\mathcal{F}$ and the sequence of **P** (*) during optimization without perturbation (*left*) and with perturbation SD = 0.6% MC (*right*).

not fit to the disturbed data as well as to the undistorted moisture content. It can also be noted that the search path differs somewhat although the starting point, $\mathbf{P}_0$, is the same. The corresponding diffusion coefficients are shown in Fig. 5 together with results from the literature (Rosenkilde and Arfvidsson 1997). In Hukka (1999) it was shown that difference between diffusion coefficients in cross-grain direction for Norway spruce and Scots pine heartwood is very small, the former being somewhat higher. This motivates the choice of comparing the results with coefficients from Rosenkilde and Arfvidsson (1997) to control the reasonableness, although samples there consisted of Scots pine tested at 60°C. A good agreement can be seen in Fig. 5 where the possible lower diffusion coefficient in Scots pine may to some extent have been cancelled by the 10°C difference between the experiment temperatures. The good accordance of the coefficient even with optimization based on distorted moisture contents is noted. To further ensure correctness of the obtained diffusion coefficient, the scheme described in Eriksson (2004) was used to compute the MC that was to be compared with measured MC. The results presented in Figs. 6 and 7 are converted from ω to moisture content in percent by use of the average dry density of the sample. In Fig. 6, the MCs in the sample are presented at six snapshots, whereas in Fig. 7, the gradual developments of the MCs at specific points are presented. It can be seen that the fit is very good. Further, even using the most perturbed data, reasonable diffusion coefficients could be extracted. This is not surprising, although the perturbation may seem to deteriorate the moisture content profiles, (see Fig. 7 (*right*); the specific choice of objective function is relatively insensible to normally distributed errors, the computed moisture contents being almost identical, (cf. Fig. 7). Finally, further information about all simulations and results are concluded in Table 1 below.

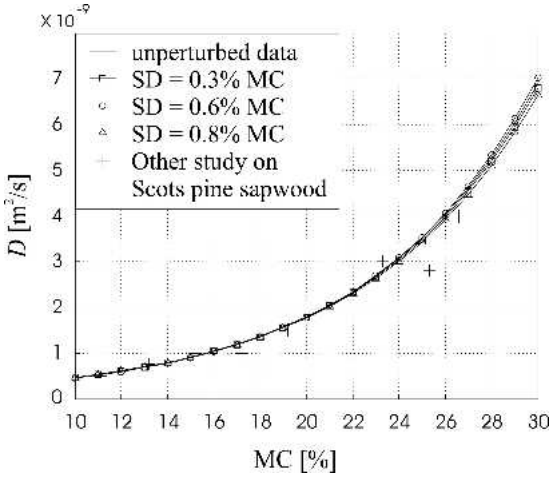

FIG. 5. The diffusion coefficient D versus the moisture content for Norway spruce sapwood in radial direction to grain. The curves are from the present study, while standalone crosses denote results from Rosenkilde and Arfvidsson (1997).

CONCLUSIONS

Experimental moisture content determination by use of X-ray CT scanning, combined with a numerical optimization procedure based on the finite element method, was used to determine the value of the radial diffusion coefficient for a sample of Norway spruce sapwood. In contrast to the ill-posed nature of inverse problems pointed out in the literature, the combined technique seems to result in a relatively robust op-

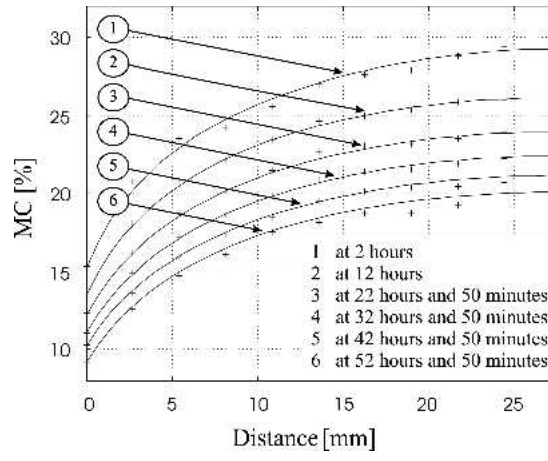

FIG. 6. The measured (cross mark) and calculated (lines) development of moisture profiles during drying of a Norway spruce sapwood sample at 50°C.

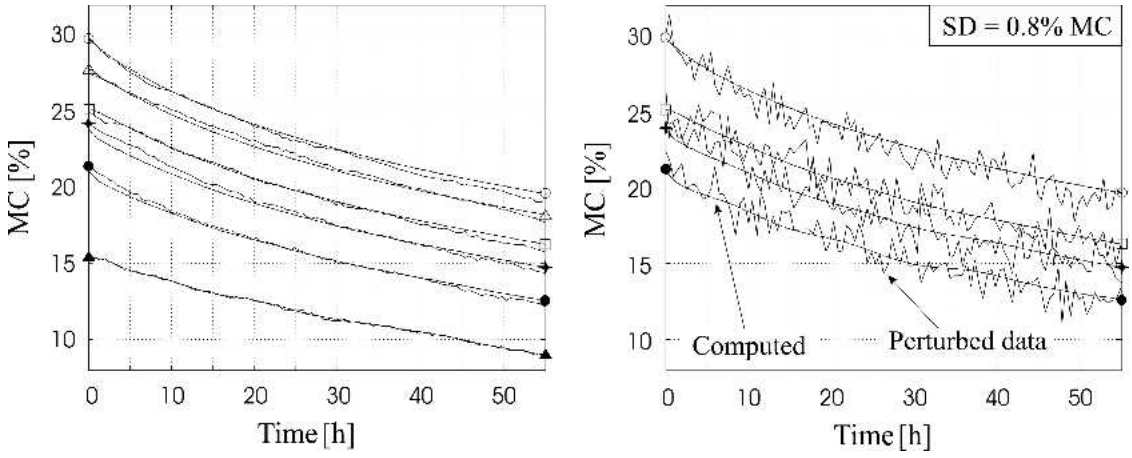

FIG. 7. The measured and calculated development of moisture content at specific points without perturbation (*left*) and with perturbation (*right*). Symbols: ○ 21.7 mm, △ 13.5 mm, □ 8.1 mm, ✣ 5.4 mm, ● 2.7 mm, ▲ 0 mm.

TABLE 1. *Prerequisites of simulations and results summary.*

Perturbation	Initial guess $\mathbf{P}_0 = [p_1, p_2]$	Stop criteria (*tol*)	$\mathbf{P}_0 = [p_1, p_2]$	$\mathcal{F}$	No. iter.
SD = 0% MC	$(5 \cdot 10^{-10}, 0.01)$	$1 \cdot 10^{-8}$	$(1.21 \cdot 10^{-10}, 0.0288)$	0.677	9
SD = 0.3% MC			$(1.22 \cdot 10^{-10}, 0.0286)$	1.620	8
SD = 0.6% MC			$(1.15 \cdot 10^{-10}, 0.0293)$	4.685	12
SD = 0.8% MC			$(1.25 \cdot 10^{-10}, 0.0282)$	7.272	11

timization procedure. The developed numerical algorithm for the determination of material parameters has the advantage of not depending on specific space and time coordinates of the measured moisture contents. Further, neither the difficult estimation of the moisture content at surface nor any assumptions concerning the surface resistance are required. The results showed that the computed diffusion coefficient agreed reasonably well with values found in the literature. Using an Arrhenius' equation type moisture content dependency of the diffusion coefficient, the calculated MCs were in good accordance with those obtained in the experiments. Based on the results presented, it can be concluded that the objective function was appropriately chosen for the currently used measurement technique, since it handles expected measurement errors in a good fashion. It is also noted that the described optimization scheme can be used to accurately study non-Fickian flows if data from successive scanning and cutting of a sample are available. Moreover, the extension of the presented scheme to multidimensional cases or other parameterizations should be straightforward. For instance, a parametrization can be applied incorporating radial (or density) dependence to study whether it significantly influences the diffusion coefficient. By replacing the diffusion model, the general idea can be used in a more complex model (e.g. phase separation) for drying above fiber saturation. Finally, it is noted that it is possible within the presented optimization scheme to compute estimates (Johansson and Runesson 2005) of how much perturbations in the measured data effect the optimal values of the material parameters.

REFERENCES

CHEN, Y., E. T. CHONG, AND D. M. WETZEL. 1996. A numerical analysis to evaluate the moisture–dependent diffusion coefficient on moisture movement during drying. Wood Fiber Sci. 28:338–345

DANVIND, J. 2003. Measuring strain and moisture content in a cross section of drying wood using Digital Speckle Photography and X-ray Computerised Tomography. *In*

Proc. 13th International Symposium on Nondestructive Testing of Wood, 19–21 August, 2002, Berkeley Campus, University of California, CA.

——— AND T. MORÉN. 2004. Using X-ray CT-scanning for moisture and displacement measurements in knots and their surroundings. *In* Proc. 5th COST ACTION E15, Advances in Drying of Wood, NAGREF/Forest Research Institute, 22–24 April, Greece.

———, J. ERIKSSON, AND H. JOHANSSON. 2004. Calibration of a constitutive model for diffusive moisture transport in wood using data from X-ray CT-scanning and Digital Speckle Photography. *In* Proc. 5th COST ACTION E15, Advances in Drying of Wood, NAGREF/Forest Research Institute, 22–24 April, Greece.

ERIKSSON, J. 2004. Study of moisture flow and moisture-induced distortions in sawn boards and laminated timber products. Lic. Thesis, Department of Structural Engineering and Mechanics, Chalmers University of Technology, Gothenburg, Sweden.

ERIKSSON, K., D. ESTEP, P. HANSBO, AND C. JOHNSON. 1996. Computational Differential Equations, Studentlitteratur, Lund, Sweden.

HUKKA, A. 1999. Diffusion and mass transfer coefficient of Nordic softwoods, Holzforschung 53:534–540.

JOHANSSON, H., AND K. RUNESSON. 2005. Parameter identification in constitutive models via optimization with a posteriori error control. Int. J. Num. Methods Eng. 62(10): 1315–1340.

KEEY, R. B., T. A. G. LANGRISH, AND J. C. F. WALKER. 2000. Kiln drying of lumber. Springer, Berlin, Germany

KLEIBER, M., H. ANTÚNEZ, T. D. HIEN, AND P. KOWALCZYK. 1997. Parameter sensitivity in nonlinear mechanics: Theory and finite element computations. John Wiley and Sons, New York, NY.

KOC, P., M. HOUŠKA, AND B. ŠTOK. 2003. Computer aided identification of the moisture transport parameters in spruce wood, Holzforschung 57:533–538.

KOPONEN, H. 1984. Dependences of moisture diffusion coefficients of wood and wooden panels on moisture content and wood properties. Paperi ja Puu 12:740–745.

LIU, J. Y., W. T. SIMPSON, AND S. P. VERRILL. 2001. An inverse moisture diffusion algorithm for the determination of diffusion coefficient, Drying Tech. 19(8):1555–1568

LUENBERGER, D. G. 2003. Linear and nonlinear programming. Kluwer Academic, London, UK.

MAHNKEN, R. 1998. Theoretiche und numeriche aspekte zur parameteridentifkation und modellierung bei metallischen werkstoffen. Report nr. f 98/2, Institut fuer Mechanik und Numeriche Mechanic, University of Hannover, Hannover, Germany.

OLEK, W., AND J. WERES. 2001. The inverse method for diffusion coefficient identification during water sorption in wood. *In* Proc. 3rd European COST E15 Workshop on Wood Drying, 11–13 June, Finland.

ROSENKILDE, A., AND J. ARFVIDSSON. 1997. Measurement and evaluation of moisture transport coefficients during drying of wood. Holzforschung 51(4):372–380.

SIMPSON, W. T., AND J. Y. LIU. 1997. An optimisation technique to determine red oak surface and internal moisture transfer coefficients during drying. Wood Fiber Sci. 29: 312–318

WADSÖ, L. 1993. Studies of water vapor transport and sorption in wood. Ph.D. thesis, Report TVBM-1013, Building Materials, Lund University, Lund, Sweden.